Acta Materialia 127 (2017) 312–318

Contents lists available at ScienceDirect

Acta Materialia

journal homepage: www.elsevier.com/locate/actamat

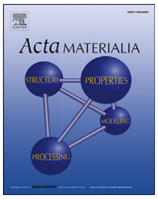

Full length article

# Segregation of solute atoms (Y, Nb, Ta, Mo and W) in $ZrB_2$ grain boundaries and their effects on grain boundary strengths: A first-principles investigation

Fu-Zhi Dai, Yanchun Zhou*, Wei Sun

*Science and Technology of Advanced Functional Composite Laboratory, Aerospace Research Institute of Materials & Processing Technology, Beijing 100076, China*

A R T I C L E I N F O

*Article history:*
Received 26 September 2016
Received in revised form
23 January 2017
Accepted 23 January 2017
Available online 25 January 2017

*Keywords:*
$ZrB_2$ based UHTCs
Grain boundary segregation
Strength
First-principles

A B S T R A C T

$ZrB_2$ based ultra-high temperature ceramics (UHTCs) exhibit a unique combination of excellent properties that makes them promising candidates for applications in extreme environments. Evaluating the correlation between microscopic defects and macroscopic performance of these materials is crucial for the design of UHTCs. The present work deals with a first-principles investigation on segregations of solute atoms (Y, Nb, Ta, Mo and W) in $ZrB_2$ grain boundaries and their influences on grain boundary strengths. Opposite segregation tendency between Y and Nb, Ta, Mo or W is obtained, where Y prefers sites with long M-B bonds, while Nb, Ta, Mo or W prefers sites with short M-B bonds. The short equilibrium M-B (M = Nb, Ta, Mo or W) bonds induce local contractions around grain boundaries, which in turn strengthens grain boundaries remarkably, thereby enhances the mechanical properties of $ZrB_2$ at evaluated temperatures. In contrast, segregation of Y poisons grain boundaries due to local expansions induced by long Y-B bonds, which will deteriorate the performance of $ZrB_2$ based UHTCs. The results provide useful guidelines for the design of $ZrB_2$ based UHTCs, since grain boundaries play a key role in determining high temperature mechanical properties.

## 1. Introduction

Recent interests in $ZrB_2$ based ultra-high temperature ceramics (UHTCs) are motivated by the development of hypersonic vehicles, in which the leading-edge and nose-tip should withstand extreme high temperature (>2000 °C) for a long service time [1–3]. Though $ZrB_2$ exhibits a unique combination of excellent properties, including high melting point, chemical inertness, effective wear and environmental resistance, its application in hypersonic technology is still impeded by poor resistance to thermal shock and oxidation [3] and rapid drop of flexural strength at high temperatures [4].

In ceramics, high temperature fracture frequently involves the nucleation, growth and coalescence of grain boundary located micro-cracks or cavities [5]. Similar mechanism also controls the failure of $ZrB_2$ based UHTCs, since the high temperature fracture is dominated by intergranular fracture [6–8]. For example, as reported by Kalish et al. [6] and Bird et al. [7] almost 90% or more grains craze by intergranular fracture at 1400 °C. Therefore, strengthening grain boundaries and suppressing grain boundary sliding are crucial in improving the high temperature performance of $ZrB_2$ based UHTCs. Previous experiments have demonstrated that $ZrB_2$ based UHTCs with additives of $TaSi_2$, $MoSi_2$, $WSi_2$ or WC generally display promising retention of strength at high temperatures [4,9–12], where evident dissolution of Ta, Mo or W into $ZrB_2$ grains has been reported [9–11]. The mechanism for the outstanding high temperature performance is still not well understood. Though segregation of solute atoms in grain boundaries has been proven a prominent way to enhance the performance of grain boundaries in many material systems, including ceramics and alloys [13–17], the interactions between solute atoms and grain boundaries in $ZrB_2$ have not been investigated until now. The present work deals with segregations of solute atoms in $ZrB_2$ grain boundaries and their influences on grain boundary strengths by first-principles calculation based on density functional theory, while it has been proved as a powerful method to evaluate the energetics, chemical or bonding state of grain boundaries [13–16]. Since the solute atoms usually result from diffusion of elements

---

* Corresponding author.
*E-mail address:* yczhou@imr.ac.cn (Y. Zhou).

http://dx.doi.org/10.1016/j.actamat.2017.01.048
1359-6454/

from additives or second phases into $ZrB_2$ during sintering, the selected solute atoms include Y, Nb, Ta, Mo and W, as guided by additives or second phases (e.g., $Y_2O_3$, $TaSi_2$, $MoSi_2$, $WSi_2$ or WC) commonly added into $ZrB_2$. The results are not only useful in understanding the outstanding high temperature performance of $ZrB_2$ ceramics with additives of $TaSi_2$, $MoSi_2$, $WSi_2$ or WC, but also valuable for further design of UHTCs.

## 2. Computational details

First-principles simulations were performed by using CASTEP [18] with exchange-correlation described by generalized gradient approximation [19]. In the simulations, Vanderbilt-type ultrasoft pseudopotential [20] was employed with cutoff energy of the plane wave being 400eV. $k$-points mesh with separation of 0.04 $Å^{-1}$ was sampled according to Monkhorst-Pack method [21] in the Brillouin zone. All of the supercells containing grain boundaries were fully optimized with respect to both lattice parameters and atom positions by using Broyden-Fletcher-Goldfarb-Shanno (BFGS) minimization scheme [22]. The tolerances for geometry optimization were set as follows: difference in total energy within $5 \times 10^{-6}$eV/atom, maximum ionic Hellmann-Feynman force within 0.01 eV/Å, maximum ionic displacement within $5 \times 10^{-4}$ Å and maximum stress within 0.02 GPa.

To assess the effects of solute atom segregation on grain boundary strengths, tensile stress-strain relations of grain boundaries were simulated. During the simulation, the supercell was incrementally deformed in the imposed strain direction. At each step, the supercell was fully relaxed by employing BFGS minimization scheme until all other stress components vanished. Then, the relaxed supercell was taken as the starting structure for the next step to ensure the stress-strain curves being continuous.

## 3. Structural models of grain boundaries

Selection of grain boundaries was guided by coincident site lattice (CSL) theory [16,23]. Three symmetrical tilt grain boundaries with their rotation axis respectively being [0001], $[11\bar{2}0]/3$ and $[01\bar{1}0]$ of $ZrB_2$ were selected. The CSL structure of each boundary is respectively shown in Fig. 1a–c with the corresponding atomic structure demonstrated in Fig. 1d–f. As illustrated in Fig. 1a, when two crystals are at a specific orientation relationship, a portion of lattice points from either lattice are coincident with each other (big, black points in Fig. 1a). Such a coincident lattice point is called a coincident site. Due to the periodic nature of both crystals, the coincident sites sometimes also form a periodic lattice (Fig. 1a), which is called CSL. In principle, exact CSL orientation relationship can only be defined by rotations around the $c$-axis for hexagonal crystals with irrational $c^2/a^2$ [16,23]. Nevertheless, near CSL structure can still be obtained for rotation axis other than $c$-axis. At this circumstance, small elastic constraints should be introduced into the system to define a constrained CSL [24]. When a CSL is defined, a supercell of the CSL can be selected to model a grain boundary. The box encircled by red and blue lines in Fig. 1a demonstrates the supercell selected to model a grain boundary. The black line represents the grain boundary position. The red crystal is located in the region enclosed by the red lines and the black line, while the blue crystal is located in the region enclosed by the blue lines and the black line. The advantage of selecting a CSL supercell to model a grain boundary is that the system naturally meets periodic boundary condition, since only periodic supercells are admissible in CASTEP. Therefore, each supercell contains two grain boundaries due to the periodic boundary condition, as demonstrated in Fig. 1d–f.

For a CSL, volume ratio between the primitive cell of the CSL to that of the crystal is defined as $\Sigma$ value of the CSL [16,23]. Then, $\Sigma$ values for boundaries in Fig. 1a–c are 7, 8 and 6, respectively. These grain boundaries will be called $\Sigma7$, $\Sigma8$, and $\Sigma6$ boundary for simplicity. For the $\Sigma7$ grain boundary, the boron-net keeps planar, which is interconnected by a sequence of 5-membered and 7-membered rings across the grain boundary, as illustrated in Fig. 1d. For the $\Sigma8$ grain boundary, the boron-net is interconnected by 8-membered rings with a shift between the 8-membered rings in adjacent layers, as demonstrated in the extracted boundary 3D structure in Fig. 1g. For the $\Sigma6$ grain boundary, the boron-net is interconnected by alternatively appeared 4-membered and 8-membered rings, as shown in Fig. 1h. Similar to the $\Sigma8$ grain boundary, the boron rings in the $\Sigma6$ grain boundary also display a relative shift between adjacent boron layers. The tilt angles, number of $ZrB_2$ cells ($N$), number of B atoms ($N_B$) and Zr atoms ($N_{Zr}$), grain boundary orientations and basis vectors of the supercells ($a$, $b$ and $c$) in either crystal are listed in Table 1. In principle, the number of $ZrB_2$ cells for each crystal combining the grain boundary should be an integral multiple of the $\Sigma$ value. However, when a boundary is constructed, some atoms may locate too close to each other, which should be deleted. As a consequence, it can be deduced from Table 1 that one Zr and two B of each crystal were deleted in the $\Sigma7$ boundary supercell and one B of each crystal was deleted in the $\Sigma8$ boundary supercell. For more details, please refer to the supplementary material.

## 4. Results and discussions

### 4.1. Grain boundary energies

The supercells were first optimized with respect to both lattice parameters and atom positions by using the BFGS minimization scheme. Lattice parameters of the supercells before and after geometrical optimization are listed in Table 2. There is no significant change in lattice parameters after optimization, which means that the adopted grain boundary models are stable. Lattice parameters with and without optimization can be adopted to estimate the elastic energy:

$$E_{\text{elastic}} = \frac{1}{2} C_{ijkl} \varepsilon_{ij} \varepsilon_{kl} V \tag{1}$$

where Einstein's notation over repeated indices is used, $C_{ijkl}$ is the fourth order elastic tensor of $ZrB_2$, $\varepsilon_{ij}$ is the elastic strain, $V$ is the volume of the supercell. The elastic strain tensor can be calculated as:

$$\varepsilon_{ij} = \frac{1}{2}\left(F_{ij} + F_{ji}\right) - \delta_{ij} \tag{2}$$

where the deformation gradient matrix $\mathbf{F}$ connects a vector before and after optimization as:

$$\boldsymbol{x}_{\text{after}} = \mathbf{F}\boldsymbol{x}_{\text{before}} \tag{3}$$

With the lattice parameters in Table 2 and lattice directions in Table 1, the elastic energy for each supercell can be calculated, and the results are listed in Table 3. The elastic constants used in the current work are $C_{11} = C_{22} = 566.4$ GPa, $C_{33} = 433.2$ GPa, $C_{44} = 253.5$ GPa, $C_{66} = 258.0$ GPa, $C_{12} = 50.4$ GPa, $C_{13} = C_{23} = 121.8$ GPa, which are consistent with values reported by others [25–27]. The transformation between the matrix form $C_{IJ}$ and fourth order tensor notation $C_{ijkl}$ of elastic constants and coordination transformation of tensors can be found in